An anti-diabetes agent protects the mouse brain from defective insulin signaling caused by Alzheimer's disease–associated Aβ oligomers

Theresa R. Bomfim,[1] Leticia Forny-Germano,[1,2] Luciana B. Sathler,[1] Jordano Brito-Moreira,[1] Jean-Christophe Houzel,[2] Helena Decker,[1,3] Michael A. Silverman,[3] Hala Kazi,[4] Helen M. Melo,[1] Paula L. McClean,[5] Christian Holscher,[5] Steven E. Arnold,[4] Konrad Talbot,[4] William L. Klein,[6] Douglas P. Munoz,[7] Sergio T. Ferreira,[1] and Fernanda G. De Felice[1]

[1]Institute of Medical Biochemistry and [2]Institute of Biomedical Sciences, Federal University of Rio de Janeiro, Rio de Janeiro, Brazil. [3]Department of Biological Sciences, Simon Fraser University, Vancouver, British Columbia, Canada. [4]Department of Psychiatry, University of Pennsylvania, Philadelphia, Pennsylvania, USA. [5]School of Biomedical Sciences, Ulster University, Coleraine, United Kingdom. [6]Department of Neurobiology and Physiology, Northwestern University, Evanston, Illinois, USA. [7]Centre for Neuroscience Studies, Queen's University, Kingston, Ontario, Canada.

Defective brain insulin signaling has been suggested to contribute to the cognitive deficits in patients with Alzheimer's disease (AD). Although a connection between AD and diabetes has been suggested, a major unknown is the mechanism(s) by which insulin resistance in the brain arises in individuals with AD. Here, we show that serine phosphorylation of IRS-1 (IRS-1pSer) is common to both diseases. Brain tissue from humans with AD had elevated levels of IRS-1pSer and activated JNK, analogous to what occurs in peripheral tissue in patients with diabetes. We found that amyloid-β peptide (Aβ) oligomers, synaptotoxins that accumulate in the brains of AD patients, activated the JNK/TNF-α pathway, induced IRS-1 phosphorylation at multiple serine residues, and inhibited physiological IRS-1pTyr in mature cultured hippocampal neurons. Impaired IRS-1 signaling was also present in the hippocampi of Tg mice with a brain condition that models AD. Importantly, intracerebroventricular injection of Aβ oligomers triggered hippocampal IRS-1pSer and JNK activation in cynomolgus monkeys. The oligomer-induced neuronal pathologies observed in vitro, including impaired axonal transport, were prevented by exposure to exendin-4 (exenatide), an anti-diabetes agent. In Tg mice, exendin-4 decreased levels of hippocampal IRS-1pSer and activated JNK and improved behavioral measures of cognition. By establishing molecular links between the dysregulated insulin signaling in AD and diabetes, our results open avenues for the investigation of new therapeutics in AD.

Introduction

Insulin resistance in peripheral tissue is a hallmark of type 2 diabetes (1). Accumulating evidence suggests that insulin resistance also develops in Alzheimer's disease (AD) brains (2). Brain levels of insulin and insulin receptor (IR) are lower in AD, and insulin signaling impairments have been documented in both postmortem analysis and in animal models of AD (3–6). Brain insulin signaling is particularly important for learning and memory (7, 8), suggesting that insulin resistance may contribute to cognitive deficits in AD.

We recently showed that soluble oligomers of the amyloid-β peptide (Aβ) instigate a striking loss of IRs from the membranes of neuronal processes (9). Aβ oligomers (AβOs) are small, diffusible aggregates that accumulate in AD brain and are recognized as potent synaptotoxins (10–12). Oligomers attach with specificity to synapses in particular neurons, acting as pathogenic ligands (13, 14). Recent studies have shown that oligomer binding induces AD-like pathology, including neuronal tau hyperphosphorylation (15), oxidative stress (16, 17), synapse deterioration and loss (13, 18), and inhibition of synaptic plasticity (19). Interestingly, insulin signaling provides a physiological defense mechanism against oligomer-induced synapse loss (13). Insulin was found to downregulate oligomer binding sites in neurons through a mechanism requiring IR tyrosine kinase activity (13). Stimulation of insulin signaling also protects neurons from oligomer-induced impairment of long-term potentiation (LTP) (20) and accumulation of hyperphosphorylated tau (21).

Understanding the molecular mechanisms accounting for impaired brain insulin signaling may illuminate new approaches to counteract neuronal damage in AD. As several pathological features, including impaired insulin signaling and inflammation, appear to be shared by patients with diabetes and those with AD, we hypothesized that, perhaps triggered by different factors, mechanisms analogous to those that account for peripheral insulin resistance in type 2 diabetes could underlie impaired brain insulin signaling in AD. Results reported here establish that insulin signaling is disrupted in Alzheimer's brains, as well as in rodent and non-human primate models of the disease, by mechanisms similar to those leading to insulin resistance in diabetes. Abnormal activation of the JNK/TNF-α pathway was verified in vivo and in

Authorship note: Theresa R. Bomfim and Leticia Forny-Germano contributed equally to this work.

Conflict of interest: William L. Klein is co-founder of Acumen Pharmaceuticals, which has been licensed by Northwestern University to develop ADDL technology for Alzheimer's therapeutics and diagnostics.

Citation for this article: *J Clin Invest.* 2012;122(4):1339–1353. doi:10.1172/JCI57256.

vitro in neurons exposed to AβOs, resulting in serine phosphorylation of IRS-1, known to block downstream insulin signaling and trigger peripheral insulin resistance in diabetes (22). Significantly, exendin-4, a new antidiabetic drug that activates pathways common to insulin signaling through stimulation of glucagon-like peptide 1 (GLP-1) receptors, blocked the impairment of insulin signaling in hippocampal cultures, reversed insulin pathology and improved cognition in Tg mice. Our findings suggest that stimulation of GLP-1 receptors (GLP1Rs) may represent a promising new approach to prevent disruption of brain insulin signaling in AD.

Results

Because serine phosphorylation of IRS-1 is a central feature in peripheral insulin resistance (22, 23), we initially looked for IRS-1pSerine in human AD brain tissue. Results demonstrate that AD brains present abnormally high levels of IRS-1 phosphorylated at serine residues 636/639 (IRS-1pSer636/639) compared with brains from non–cognitively impaired (NCI) subjects (Figure 1, A–C, and Supplemental Table 1; supplemental material available online with this article; doi:10.1172/JCI57256DS1), in line with a recent study that examined other pSer epitopes (4). In NCI controls, IRS-1pSer636/639 immunoreactivity was almost exclusively detectable in cell nuclei, appearing as puncta of variable sizes (Figure 1A). In some cases, extranuclear immunoreactivity in neuronal cell bodies was also detected, but this was rare in subjects younger than 75 years. In contrast, in AD patients a high density of neurons with IRS-1pSer636/639 labeling in cell bodies and, occasionally, in proximal dendrites was found from the earliest ages studied (i.e., 51 years). This was most conspicuous in the hippocampal CA1 region (Figure 1B). In 20 of 22 (91%) age- and sex-matched pairs of AD and control cases, the density of CA1 neurons with extranuclear IRS-1pSer636/639 labeling was greater in the AD case (Wilcoxon signed-ranks test; $W = 239$, $P = 0.0001$; Figure 1C and Supplemental Table 1). Control specificity tests on the IRS-1pSer636/639 antibody showed that labeling in AD brain could be fully blocked by competition with synthetic phosphorylated immunogen (Supplemental Figure 1), but not with the corresponding non-phosphorylated peptide. These findings are in harmony with peripheral mechanisms leading to type 2 diabetes and support the idea that AD is characterized by CNS insulin resistance.

Memory impairment in AD is now attributed, at least in part, to the synaptotoxicity of AβOs (12, 13, 19, 24), which accumulate in AD brains (14) and in animal models of AD (25). Recent studies have implicated oligomers in neuronal insulin resistance (9, 13). Thus, we next investigated whether pathological IRS-1pSer could develop from the neuronal impact of AβOs. Using highly differentiated hippocampal neuronal cultures, we found that AβOs induced abnormal elevation in somatodendritic IRS-1pSer636 levels (Figure 1, D–F). These results provide a salient pathogenic basis to account for elevated IRS-1pSer levels in AD brains. Because phosphorylation of IRS-1 at additional serine residues (other than Ser636) is also known to account for insulin resistance in peripheral tissue (23, 26), we searched for neuronal IRS-1 phosphorylation at other epitopes. We found that IRS-1pSer616, IRS-1pSer312, and IRS-1pSer307 levels were also increased in hippocampal neurons exposed to AβOs (Figure 1, F and M). In parallel, and consistent with the expected insulin resistance associated with serine phosphorylation of IRS-1, oligomers inhibited physiological IRS-1 phosphorylation at tyrosine residue 465 (IRS-1pTyr465; Figure 1, G–I), an essential step in the IR-stimulated signaling pathway. Neurons targeted by AβOs exhibited increased IRS-1pSer levels, whereas non-attacked neurons showed low IRS-1pSer levels, as illustrated in Figure 1, J–L. Dysregulation of IRS-1 signaling, which we found to be prominent in AD brains (Figure 1B), is thus instigated by AβOs in central neurons.

Neuronal cultures used throughout our study were maintained in Neurobasal medium supplemented with B-27, an insulin-containing supplement, considered optimal conditions to preserve synapse health and function and to grow mature hippocampal cultures (27). In order to determine whether the increase in IRS-pSer described above might be related to insulin coming from B-27, we used cultures grown in insulin-free B-27. As shown in Supplemental Figure 2, in insulin-free medium AβOs triggered very similar increases in IRS-1pSer levels. Results thus establish that IRS-1pSer is specifically triggered by oligomers rather than by a possible physiological action of insulin present in B-27.

To determine whether the insulin signaling defect found in cell culture experiments also occurs in vivo, we investigated the effect of AβOs on IRS-1pSer in the brains of non-human primates. To this end, 3 adult cynomolgus monkeys (*Macaca fascicularis*) received intracerebroventricular (i.c.v.) injections of oligomers. A sham-operated monkey was used as a control. Remarkably, we found that the monkeys that received i.c.v. oligomer injections presented elevated levels of neuronal IRS-1pSer636 in the hippocampus compared with the control monkey (Figure 2, A–G). Interestingly, IRS-1pSer636 levels were also increased in the temporal cortex of monkeys that received injections of AβOs, indicating that the impact of oligomers on IRS-1 signaling extends to other brain regions in addition to the hippocampus (Supplemental Figure 3). These results demonstrate that AβOs instigate elevated serine phosphorylation of IRS-1 in the brains of monkeys, establishing the in vivo and in situ relevance of our findings.

We next examined IRS-1pSer levels in the brains of APPSwe,PS1ΔE9 (APP/PS1) mice, which express transgenes for human amyloid precursor protein (APP) bearing the Swedish mutation and a deletion mutant form of presenilin 1. IRS-1pSer636 and IRS-1pSer312 levels, but not IRS-1pSer307 levels, were increased in hippocampi of APP/PS1 Tg mice compared with WT mice (Figure 2H).

Non-phosphopeptide antibodies were used to detect total levels of IRS-1 and IRS-2 in our experimental models. We noted that distinct patterns of dendritic labeling were obtained for IRS-1 and IRS-2 (Figure 3, A, B, F, and G). No differences in total IRS-1 levels were observed in oligomer-treated cultures or in hippocampi of APP/PS1 mice (Figure 3, A–E). In contrast, total IRS-2 levels increased in hippocampal cultures exposed to AβOs, as revealed by both immunocytochemistry and Western blot analysis (Figure 3, F–I). This impact of oligomers may be related to the fact that IRS-2 is a negative regulator of memory formation, as shown by recent studies (28, 29). However, IRS-2 levels were significantly decreased in APP/PS1 Tg mice compared with WT mice (Figure 3J). Decreased levels of IRS-2 have also been found in AD brains (4), suggesting that chronic exposure to AβOs may give rise to a compensatory mechanism aimed to decrease the negative impact of brain IRS-2 signaling on memory.

Previous studies have linked IRS-1 serine phosphorylation to JNK activation in diabetes and in obesity-related insulin resistance (22). In peripheral tissue, IRS-1 is phosphorylated at Ser636 by p-JNK (30). This prompted us to investigate the involvement of JNK in oligomer-induced IRS-1pSer in cell culture experiments. AβOs

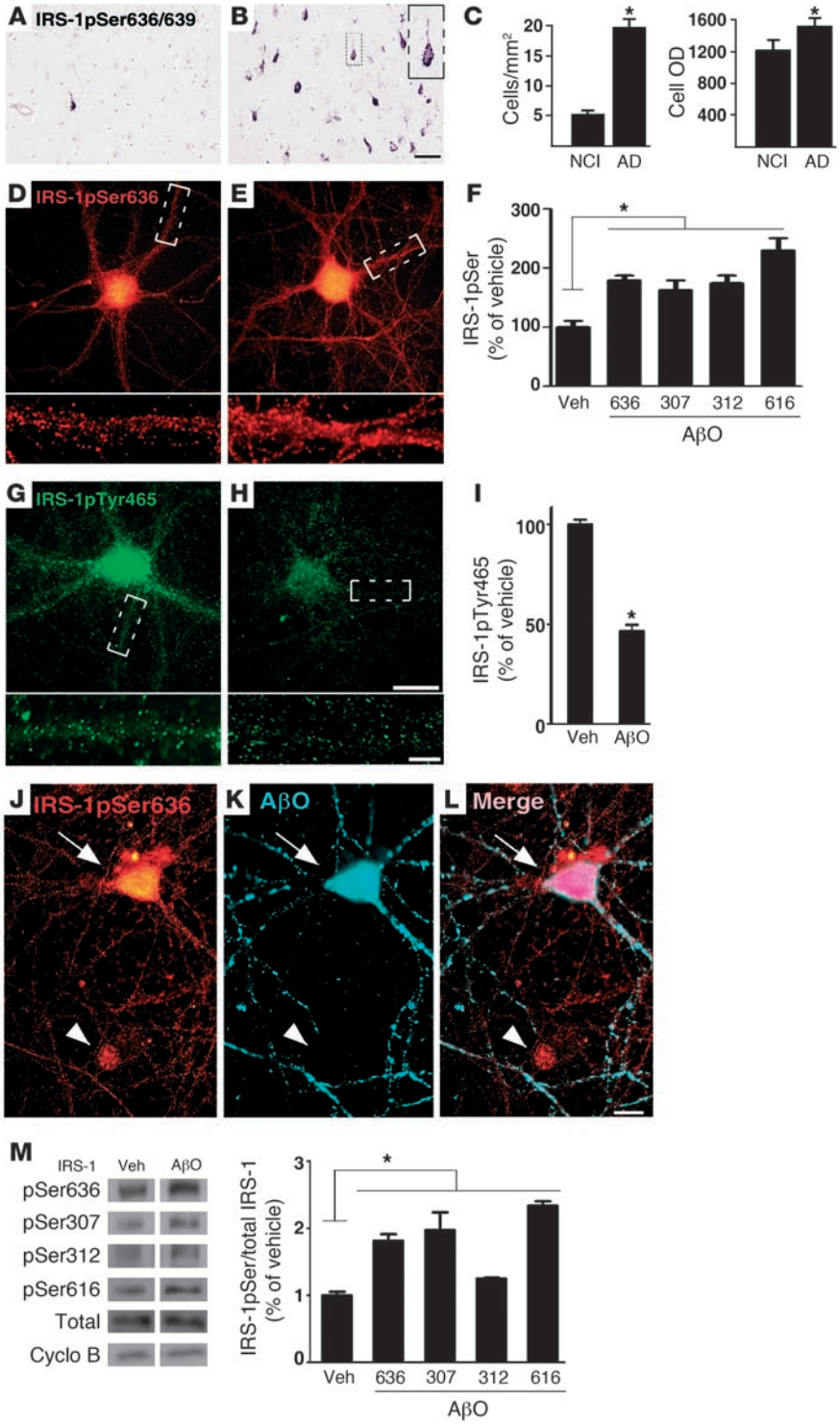

Figure 1

IRS-1pSer is increased in AD brain and in hippocampal neurons exposed to AβOs. Higher density of IRS-1pSer636/639–positive neurons in CA1 hippocampal region from a 68-year-old AD patient (**B**) compared with a 73-year-old NCI control (**A**). IRS-1pSer636-639 in AD sometimes extends into apical dendrites (inset in **B**; scale bar: 20 μm). (**C**) In 22 matched pairs, AD patients presented a higher density of IRS-1pS636/639–positive cells and mean optical density (OD) of IRS-1pSer636-639 labeling/cell than NCI individuals ($P = 0.0001$). IRS-1pSer636 (**D** and **E**) or IRS-1pTyr465 (**G** and **H**) immunolabeling in hippocampal neurons exposed to vehicle (**D** and **G**) or 500 nM AβOs (**E** and **H**) for 3 hours (scale bar: 50 μm). Boxes under each panel show optical zoom images of selected dendrite segments (white dashed rectangles; scale bar: 10 μm). (**F**) Integrated IRS-1pSer and (**I**) IRS-1pTyr465 immunofluorescence levels determined from 4–8 experiments (independent cultures, 30 images analyzed/experimental condition/experiment). Veh, vehicle. (**J** and **L**) Representative images showing elevated IRS-1pSer636 (red, **J**) in a neuron targeted by AβOs (NU4 oligomer-specific antibody labeling; cyan, **K**, white arrow). (**L**) Merged image reveals a cell not attacked by AβOs (white arrowhead) with low IRS-1pSer636 levels. (**M**) Western blots of hippocampal cultures exposed to vehicle or 500 nM AβOs for 3 hours. Lanes were run on the same gel but were noncontiguous. Graph shows densitometric analysis for IRS-1pSer epitopes normalized by total IRS-1 level. Cyclophilin B (Cyclo B) was used as an additional loading control. *$P < 0.05$, ANOVA followed by Bonferroni post-hoc test, relative to vehicle-treated cultures.

failed to induce IRS-1pSer in hippocampal neurons transfected with GFP-fused dominant negative JNK (DN JNK; Figure 4, A–D), indicating a role for JNK in neuronal insulin resistance. As a control, mock transfection with a plasmid containing only GFP had no protective effect (Figure 4C). Oligomer-induced accumulation of IRS-1pSer636 was also blocked by the pharmacological JNK inhibitor SP600125 (Figure 4, E–G and I). Moreover, oligomer-induced JNK activation was directly observed in hippocampal neuronal cultures (Figure 4J). Consistent with the involvement of JNK indicated by our results, a recent study showed that AβOs induce tau hyperphosphorylation and IRS-1 inactivation via JNK activation (31).

Subsequently, we sought to determine whether p-JNK levels were elevated in the brains of APP/PS1 mice. We found a 4-fold increase in p-JNK levels in hippocampi of Tg mice compared to WT animals (Figure 4K), demonstrating that activation of JNK, first detected in cell culture experiments, occurs in vivo. No changes in

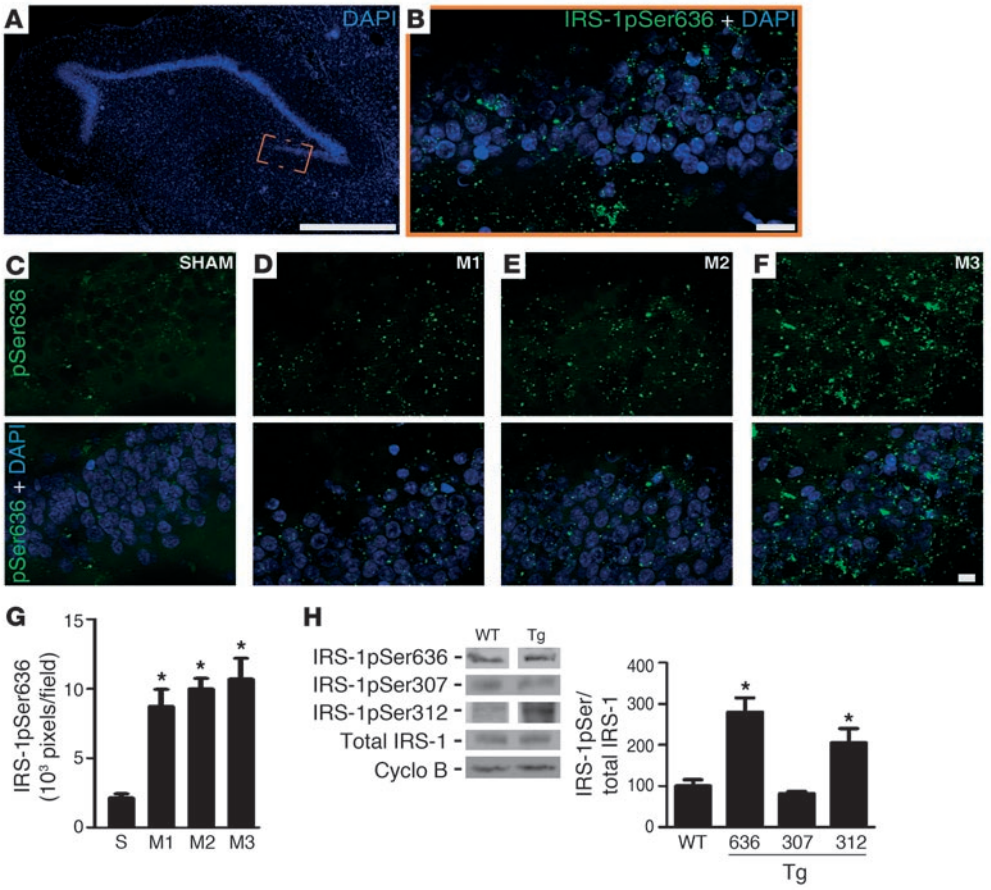

Figure 2

Elevated IRS-1pSer levels in the hippocampi of cynomolgus monkeys that received i.c.v. injections of AβOs and in APP/PS1 Tg mice. (**A** and **B**) Photomontage reconstruction of the hippocampus of a monkey that received i.c.v. injections of AβOs. The dashed rectangle indicates a region in the dentate gyrus that is shown enlarged in **B**, revealing IRS-1pSer636 immunoreactivity (green). DAPI staining is in blue. (**C**–**F**) IRS-1pSer636 immunoreactivities in the same segments of dentate gyri from a control (sham-operated) monkey (**C**) and 3 different monkeys that received injections of AβOs (**D** and **F**). Scale bars: 500 μm (**A**), 20 μm (**B**), 50 μm (**C**–**F**). (**G**) IRS-1pSer636 immunolabeling density (see Methods) from 20–31 images acquired in dentate gyri of sham-operated (S) or AβO-injected monkeys (M1–M3). *P < 0.001, ANOVA followed by Bonferroni post-hoc test, relative to sham-operated monkey. (**H**) Representative blots of IRS-1pSer636, IRS-1pSer307, and IRS-1pSer312 in hippocampi of APP/PS1 Tg mice. Lanes for IRS-1pSer636 and pSer312 were run on the same gel but were noncontiguous. Graph shows densitometric quantification of IRS-1pSer levels in Tg (n = 7) or WT mice (n = 5) normalized by total IRS-1 levels. Cyclophilin B was used as an additional loading control. *P < 0.02, Student's t test, compared with WT.

levels of total JNK were found in hippocampal cultures exposed to oligomers or in hippocampi of APPS/PS1 Tg mice (Supplemental Figure 4). Future studies employing mice with knockout of IRS-1, JNK1/2, or JNK3 may provide additional insight into the mechanistic links between insulin resistance and AD.

In peripheral insulin resistance, JNK activity is known to be stimulated by TNF-α signaling (22), and TNF-α levels are elevated in AD (32). Interestingly, we found that abnormal IRS-1pSer636 triggered by AβOs was completely blocked by infliximab, a TNF-α neutralizing antibody (Figure 4, H and I). We further detected an increase in TNF-α levels in concentrated conditioned medium from hippocampal cultures exposed to AβOs (Figure 4L). No differences were found in levels of TNF-α receptor in cultured neurons exposed to oligomers or in hippocampi of Tg mice (Figure 4, M and N). The results suggest that oligomer-induced elevation in proinflammatory TNF-α levels triggers aberrant activation of JNK and, ultimately, serine phosphorylation of IRS-1.

We next analyzed levels of p-JNK in AD brains and found that the density of neurons with detectable levels of activated JNK was significantly increased in AD hippocampi (Figure 5, A–D), giving strong support to our proposal that activation of the JNK pathway plays a key role in AD pathology. Finally, we examined JNK activation in the brains of cynomolgus monkeys. Consistent with elevated IRS-1pSer levels, the 3 monkeys that received i.c.v. injections of AβOs presented elevated neuronal p-JNK levels in their hippocampi compared with the sham-operated monkey (Figure 5, E–I). Both cytoplasmic and nuclear p-JNK labeling were detected in NeuN-positive cells, but not in GFAP-positive cells (Figure 5, J–L), demonstrating neuronal specificity of JNK activation induced by oligomers. These results establish that abnormal activation of neuronal JNK is triggered by AβOs in the brains of non-human primates and support a key role of JNK in neuronal insulin resistance in AD.

Aberrant activation of JNK has been linked to impaired axonal transport in neurological disorders (33). Several neurodegenera-

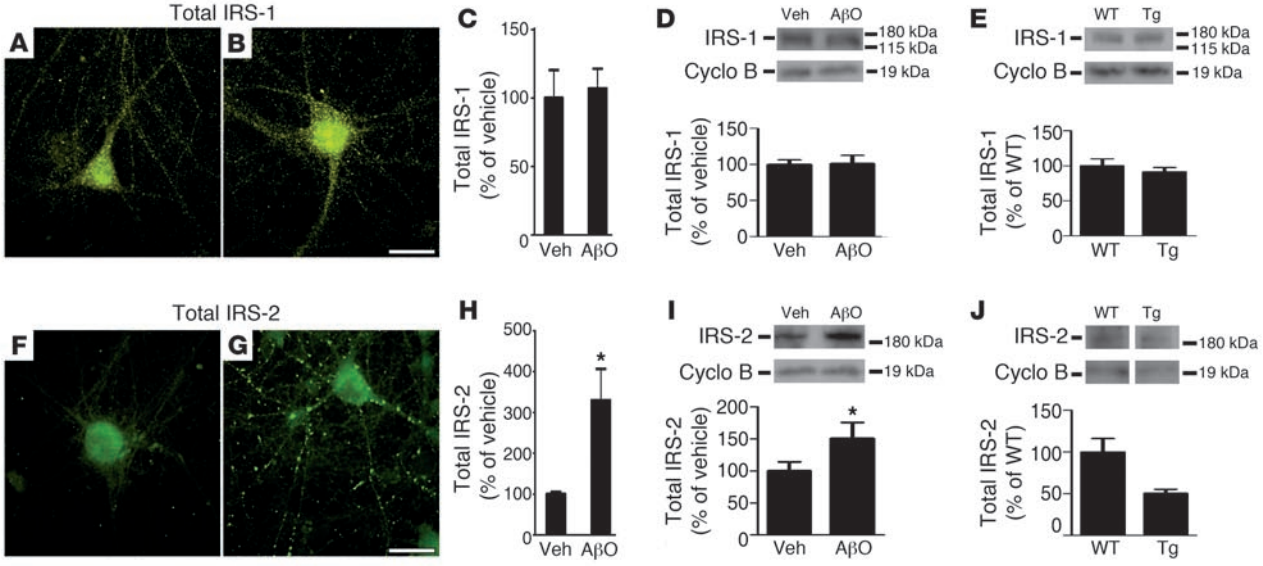

Figure 3

IRS-1 and IRS-2 levels in mature hippocampal neuronal cultures exposed to AβOs and in the hippocampi of Tg mice. Representative immunofluorescence images of total IRS-1 and total IRS-2 levels in hippocampal neurons exposed to vehicle (**A** and **F**) or 500 nM AβOs (**B** and **G**) for 3 hours. Graphs show integrated immunofluorescence levels of total IRS-1 (**C**) or IRS-2 (**H**). Results are from 3 experiments using independent cultures (20 images analyzed per experimental condition per culture). **P* < 0.001, Student's *t* test, relative to vehicle-treated cultures. Scale bars: 50 μm. (**D** and **I**) Immunoblots for total IRS-1 and IRS-2 levels in hippocampal neurons exposed to vehicle or 500 nM AβOs for 3 hours. Graphs show densitometric quantification of IRS-1 (**D**) and IRS-2 (**I**) levels normalized by cyclophilin B. (**E** and **J**) Total IRS-1 and IRS-2 levels, respectively, in hippocampal homogenates from APP/PS1 Tg ($n = 7$) or WT mice ($n = 5$). Lanes for IRS-2 (**J**) were run on the same gel but were noncontiguous. Graphs show densitometric quantification of IRS-1 or IRS-2 levels normalized by cyclophilin B immunoreactivity. **P* < 0.05, Student's *t* test, relative to vehicle-treated cultures.

tive diseases, including AD, display axonal pathologies comprising defective transport and abnormal accumulation of proteins and organelles (34). Because AβOs were recently shown to impair axonal transport in hippocampal neurons (35), we further asked whether oligomer-induced JNK activation might be responsible for defects in axonal transport of dense core vesicles (DCVs) (see Supplemental Figure 5 for a scheme describing axonal transport measurements). Significantly, the JNK inhibitor SP600125 blocked axonal transport alterations induced by oligomers (Figure 6, Supplemental Table 2, and Supplemental Video 1), implicating JNK activation in impaired axonal transport in AD.

Double-stranded RNA-dependent protein kinase (PKR) and IκB kinase (IKK) are two stress-sensitive kinases that mediate serine phosphorylation of IRS-1 and are critical regulators of peripheral insulin resistance (36–39). In an additional set of experiments, we examined whether PKR and/or IKK were also activated by AβOs. A selective PKR inhibitor completely blocked oligomer-induced IRS-1pSer636, IRS-1pSer312, and IRS-1pSer307 in hippocampal cultures (Figure 7, A–L). IKK was also found to be involved in oligomer-induced IRS-1pSer, as acetylsalicylic acid completely prevented abnormal IRS-1pSer636 (Figure 7, M–O and Q). Abnormally activated mTOR signaling has also been implicated in peripheral insulin resistance (40). However, the mTOR inhibitor rapamycin had no effect on IRS-1pSer636 triggered by oligomers (Figure 7, P and Q), suggesting that mTOR is not involved in oligomer-induced serine phosphorylation of IRS-1. The involvement of PKR and IKK in AβO-induced IRS-1pSer provides additional evidence for a close parallelism between inflammation-associated brain insulin resistance in AD and chronic inflammation-induced insulin resistance in peripheral tissues in type 2 diabetes.

Stimulation of brain insulin signaling has been suggested as a promising approach to prevent synapse deterioration and memory decline in AD (41, 42). We thus next tested whether bolstering insulin signaling might also protect neurons from aberrant activation of the JNK/IRS-1pSer pathway triggered by AβOs. We examined the effects of insulin and exendin-4 (exenatide), an incretin hormone analog that activates the insulin signaling pathway through GLP1R stimulation (43) and has been recently approved for treatment of diabetes. GLP1Rs are present and functional in cultured neurons as well as in rodent and human brains, and emerging evidence indicates that their stimulation regulates neuronal plasticity and cell survival (44). Significantly, we found that both insulin and exendin-4 prevented the increase in IRS-1pSer636 (Figure 8, A–D) and the decrease in IRS-1pTyr465 levels (Figure 8, E–H) induced by oligomers. Exendin 9-39, a potent GLP1R antagonist and a competitive inhibitor of exendin-4, blocked the protective action of exendin-4, demonstrating that protection was specifically mediated by activation of GLP1Rs (Figure 8D). Because neuronal cultures used in our study were maintained in Neurobasal B-27, an insulin-containing supplement, it is possible that these results reflect to some extent crosstalk between exendin signaling and signaling initiated by insulin. Control experiments showed that exendin-4 or insulin alone (i.e, in the absence of oligomers) had no significant effects on IRS-1pSer levels (Figure 8D). Interestingly, insulin and exendin-4 also protected neurons from the above-described oligomer-induced impairment of axonal transport (Figure 8, I and J, Supplemental Tables 2 and 3, and Supplemental Videos 2 and 3). Because JNK dysregula-

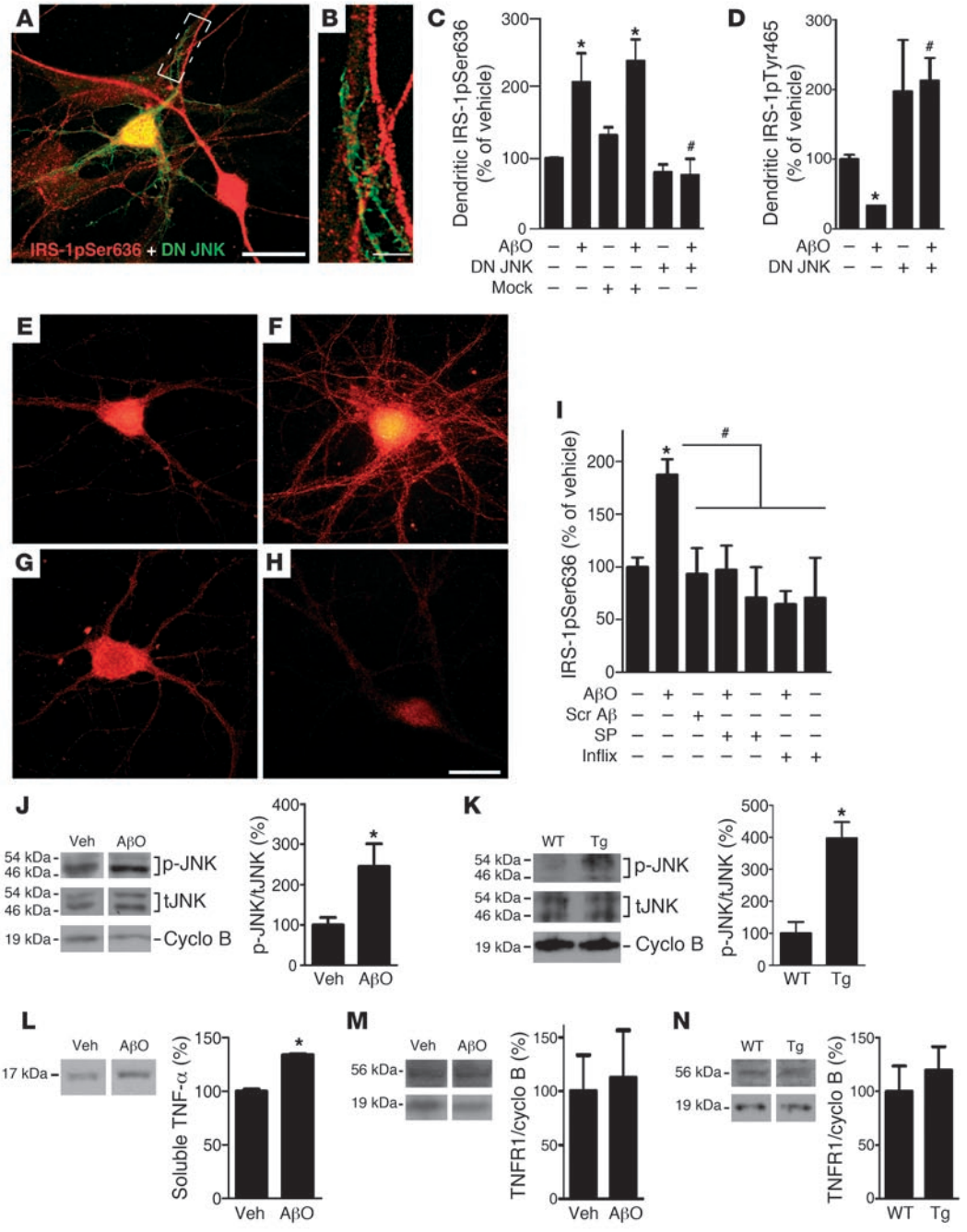

Figure 4

JNK mediates AβO-induced IRS-1pSer. (**A**) Representative image showing low IRS-1pSer levels (red) in a hippocampal neuron transfected with GFP-fused DN JNK (green; scale bar: 50 μm). (**B**) Higher-magnification image of dendrite segment (white box in **A**; scale bar: 10 μm). (**C** and **D**) integrated IRS-1pSer636 and IRS-1pTyr465 immunofluorescence levels, respectively. *$P < 0.001$ relative to vehicle-treated cultures, #$P < 0.001$ relative to AβO-exposed cultures; ANOVA followed by Bonferroni post-hoc test. (**E**–**H**) Hippocampal neurons exposed for 3 hours to vehicle (**E**), 500 nM AβOs (**F**), 10 μM SP600125 (SP) plus 500 nM AβOs (**G**), or 1 μg/ml infliximab (Inflix) plus 500 nM AβOs (**H**). Scale bar: 50 μm. (**I**) Integrated IRS-1pSer immunofluorescence levels determined from 4 experiments (independent cultures, 20 images analyzed/experimental condition/experiment). *$P < 0.001$ relative to vehicle-treated cultures, #$P < 0.001$ relative to AβO-exposed cultures; ANOVA followed by Bonferroni post-hoc test. Scr, scrambled $Aβ_{1–42}$ peptide. (**J**) Immunoblot of p-JNK in cultures exposed to 500 nM AβOs for 3 hours. (**K**) p-JNK levels in hippocampal homogenates from APP/PS1 Tg or WT mice. tJNK, total JNK. (**L**) TNF-α immunoblot in concentrated conditioned medium from cultures exposed to AβOs for 3 hours. (**M** and **N**) TNF-α receptor levels in cultures exposed to 500 nM AβOs for 3 hours and in hippocampal homogenates from APP/PS1 Tg ($n = 7$) or WT mice ($n = 5$), respectively. (**M** and **N**) Densitometric quantification normalized by cyclophilin B. Lanes in **J** and **L**–**N** were run on the same gel but were noncontiguous. *$P < 0.02$, Student's t test.

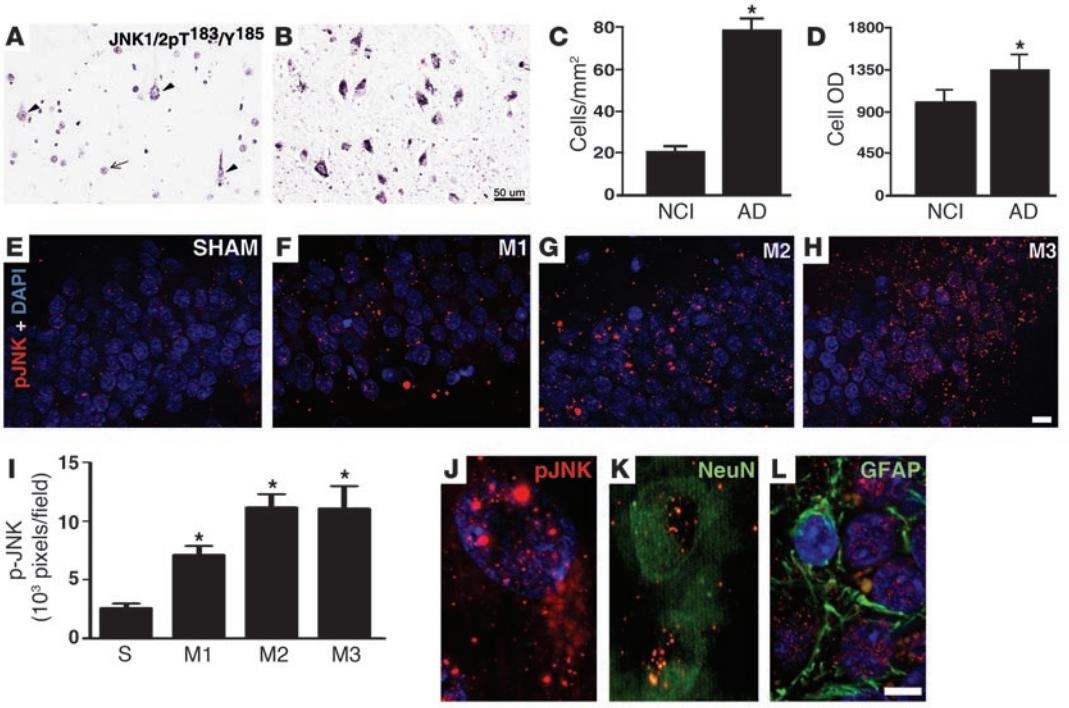

Figure 5

Elevated p-JNK levels in AD brains and in hippocampi of cynomolgus monkeys that received i.c.v. injections of AβOs. (**A**–**D**) Density of neurons in the same segment of hippocampal field CA1 with detectable JNK1/2pT183/pY185 in NCI controls (**A**) or AD patients (**B**). In control cases (**A**), immunoreactivity for p-JNK is generally limited to portions of cell nuclei (arrow), with only a small number of neurons showing immunoreactivity in the cytoplasm (arrowheads). Neurons with detectable cytoplasmic JNK1/2 pT183/pY185 also showed increased levels of this activated protein in AD (**B** and **C**) as indicated by higher mean OD in AD than in control samples (**D**). Graphs show mean values ± SD for neurons throughout CA1 in 22 matched pairs of control and AD cases. *$P < 0.0001$ relative to NCI individuals. (**E**–**H**) p-JNK immunoreactivities in the same segments of the dentate gyri from a sham-operated monkey (**E**) and 3 different monkeys that received i.c.v. injections of AβOs (**F**–**H**). (**I**) p-JNK immunolabeling density determined (see Methods) from 20–33 images acquired from dentate gyri of sham (S) or oligomer-injected monkeys (M1–M3). *$P < 0.001$ relative to the sham-operated monkey, ANOVA followed by Bonferroni post-hoc test. **J**, **K**, and **L**, enlarged images demonstrating both cytoplasmic and nuclear p-JNK labeling (**J**) of NeuN-positive cells (**K**). (**L**) p-JNK immunoreactivity was not associated with GFAP-positive cells. Scale bars: 50 μm (**A**, **B**, and **E**–**H**); 5 μm (**J**–**L**).

tion appears to underlie axonal transport defects in a number of neurodegenerative disorders in addition to AD (33), this raises the possibility that prevention of aberrant JNK activation by bolstering insulin signaling might be beneficial in such disorders.

Protection by insulin against AβO-induced neuronal damage has been shown to involve downregulation of oligomer binding sites (13). Additional experiments thus aimed to determine whether exendin-4 also interferes with oligomer binding to neurons. Results showed that exendin-4 did not block oligomer binding (Supplemental Figure 6). Along with the results presented above, this indicates that GLP1R activation by exendin-4 prevents oligomer-induced impairment in IRS-1 signaling even when oligomers are attached to neurons. We also determined GLP1R levels in AβO-treated neuronal cultures and in hippocampi of AD Tg mice. No changes in levels of GLP1R were found in hippocampal cultures exposed to oligomers or in hippocampi of APPS/PS1 Tg mice (Supplemental Figure 7). Because brain insulin signaling may decline with aging and in AD (45), exendin-4 may thus be more efficient than insulin in protecting neurons from the toxic impact of oligomers.

Finally, since exendin-4 readily crosses the blood-brain barrier and has been shown to facilitate hippocampal synaptic plasticity and cognition (44, 46, 47), we asked whether systemic administration of a GLP1R agonist could enhance brain insulin signaling in APP/PS1 mice. Mice (13–14 months of age) were treated for 3 weeks with a daily intraperitoneal injection of exendin-4 (48). Exendin-4–treated mice exhibited significant reductions in brain levels of IRS-1pSer636, IRS-1pSer312, and p-JNK compared with vehicle-treated animals (Figure 8, K and L). Interestingly, spatial memory in the Morris water maze task was improved by chronic exendin-4 administration to Tg mice. Exendin-4–treated APP/PS1 mice learned the task faster, with significantly reduced escape latencies observed on days 3 and 4 of training, compared with saline-treated mice (Figure 8, M and N). Furthermore, exendin-4–treated mice had improved memory retention, as indicated by a significantly longer time spent in the target quadrant during the probe trial conducted 24 hours after the last training session (Figure 8O). These data demonstrate the beneficial effect of exendin-4 on cognition in AD Tg mice. Interestingly, we further found that treatment with exendin-4 entailed reductions in brain levels of amyloid plaque load and soluble Aβ in the cerebral cortices of AD Tg mice (Figure 8, P–R).

Reported effects of peripheral exendin-4 administration include reduced plasma glucose levels and decreased food intake and body weight, and these could mimic the anti-aging effects of

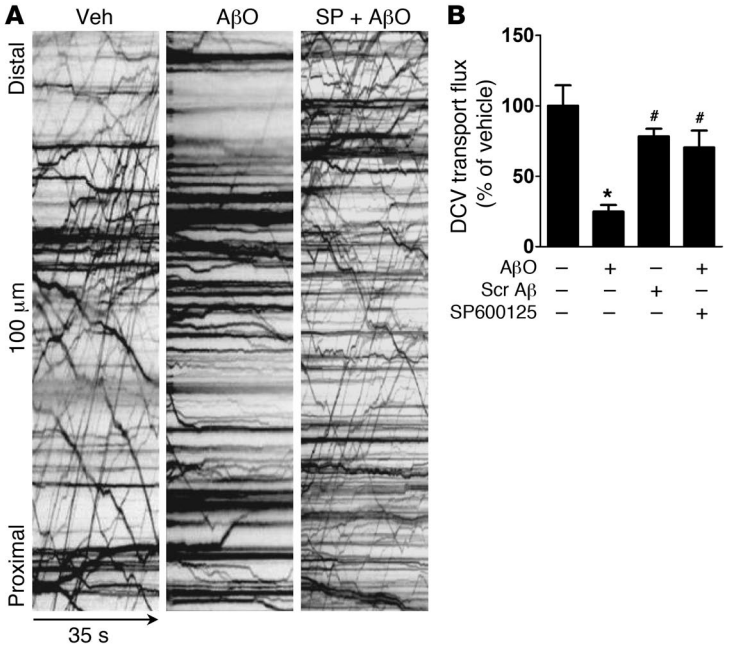

Figure 6
JNK mediates oligomer-induced impairment of axonal transport of DCVs in hippocampal neurons. (**A**) Representative kymographs comparing axonal DCV transport in neurons exposed to vehicle, 500 nM AβOs, or 10 μM SP600125 plus 500 nM oligomers for 18 hours. (**B**) Quantification of total DCV transport flux. A minimum of 15 cells per condition from at least 2 independent cultures were analyzed. Transport parameters (organelle flux, velocity, run length) of DCVs were extracted from quantitative analysis of kymograph traces (see Methods). $^{*}P < 0.001$ relative to vehicle-treated cultures; $^{\#}P < 0.001$ relative to cultures exposed to AβOs.

caloric restriction. We note that, for the duration of the behavioral experiments described above, comparable and slight weight losses were observed in all groups of mice analyzed, regardless of whether they received daily intraperitoneal injections of exendin-4 or saline (Supplemental Figure 8). This may be due to the exercise regime to which the animals were subjected during training and trials in the Morris water maze. We also note that, in insulin-secreting cells, exendin-4 inhibits JNK activation (49), counteracts TNF-α–mediated apoptosis, and reverses inhibition of the IRS-1 pathway (50). Taken together, our results suggest that exendin-4 restored impaired brain insulin signaling, decreased plaque load and soluble Aβ levels, and improved learning and memory.

Discussion

Recent studies have shown that type 2 diabetes increases the risk of AD (51), and a newly recognized form of brain insulin resistance has been connected to AD (2, 3). Here, we describe a pathogenic mechanism by which a type of "brain diabetes" is triggered by AβOs, synaptotoxins that accumulate in AD brains. Because brain insulin signaling is centrally involved in learning and memory (8), the impact of AβOs on brain insulin signaling may be a mechanism potentially contributing to early memory loss in AD.

Similar to mechanisms that cause peripheral insulin resistance in type 2 diabetes, our results show that AβOs induce neuronal insulin resistance by activating TNF-α and the stress kinases JNK, IKK, and PKR, leading to serine phosphorylation of IRS-1 (Figure 9A). Analysis of AD brains confirmed abnormal phosphorylation of IRS-1 at Ser636/639, which is typically associated to peripheral insulin resistance in diabetes (1). IRS-1pSer redistribution was recently reported in AD brains (31). Because we have previously shown that AβOs internalize/redistribute neuronal IRs (9, 13), it is possible that IR loss may underlie, or facilitate, IRS-1pSer increases. This is consistent with our finding that insulin, previously shown to block IR downregulation induced by AβOs (13), further blocks IRS-1pSer.

In peripheral insulin resistance, IRS-pSer is a major target for phosphorylation by mTOR (40, 52, 53). In contrast, the mechanism by which oligomers trigger neuronal IRS-1 inhibition does not appear to involve mTORC1 activation, as rapamycin had no protective effect against IRS-1pSer. The possible role of mTOR in AD is still controversial. mTOR activity was shown to be increased in brains of 3xTg-AD mice (54) and rapamycin improved cognition in PDAPP Tg mice (55, 56). On the other hand, upregulating mTOR signaling rescued LTP in another AD mouse model (Tg2576), suggesting that mTOR inhibition correlates with impaired synaptic plasticity in AD (57). Other studies have shown that mTOR signaling is downregulated in cellular and animal models of AD (54, 58). Given these controversial literature reports, further studies aimed at unraveling the possible role of mTOR signaling in AD appear warranted.

We found significant increases in p-JNK levels in AD brains and in hippocampi of APP/PS1 Tg mice. Using a different strain of Tg mice fed a high-fat diet, a recent study reported abnormally elevated brain levels of activated JNK (31). Remarkably, elevated IRS-1pSer636 and p-JNK levels were triggered by injection of AβOs in the brains of monkeys. Considering the dearth of animal model systems that truly recapitulate the main features of AD (59), a monkey model of AD may provide insight into central aspects of pathology that could be present exclusively in primates.

Inflammation is an important mediator of insulin resistance in obesity and diabetes (23, 26, 60, 61). Supporting the notion that AβO-induced neuronal insulin resistance derives from an inflammatory response mediated by TNF-α, the TNF-α–blocking antibody infliximab protected neurons against oligomers. Used to treat inflammatory diseases (62), infliximab and etanercept, a TNF-α–blocking recombinant protein, have been proposed as novel therapeutic agents to combat insulin resistance in type 2 diabetes (63) and memory decline in AD (64). By defending neurons from oligomer-induced dysregulation of insulin signaling, infliximab treatment may constitute a novel approach to prevent memory impairment in AD.

We did not observe significant changes in levels of IRS-1pSer307 in hippocampi from AD Tg mice, while in cultured neurons AβOs

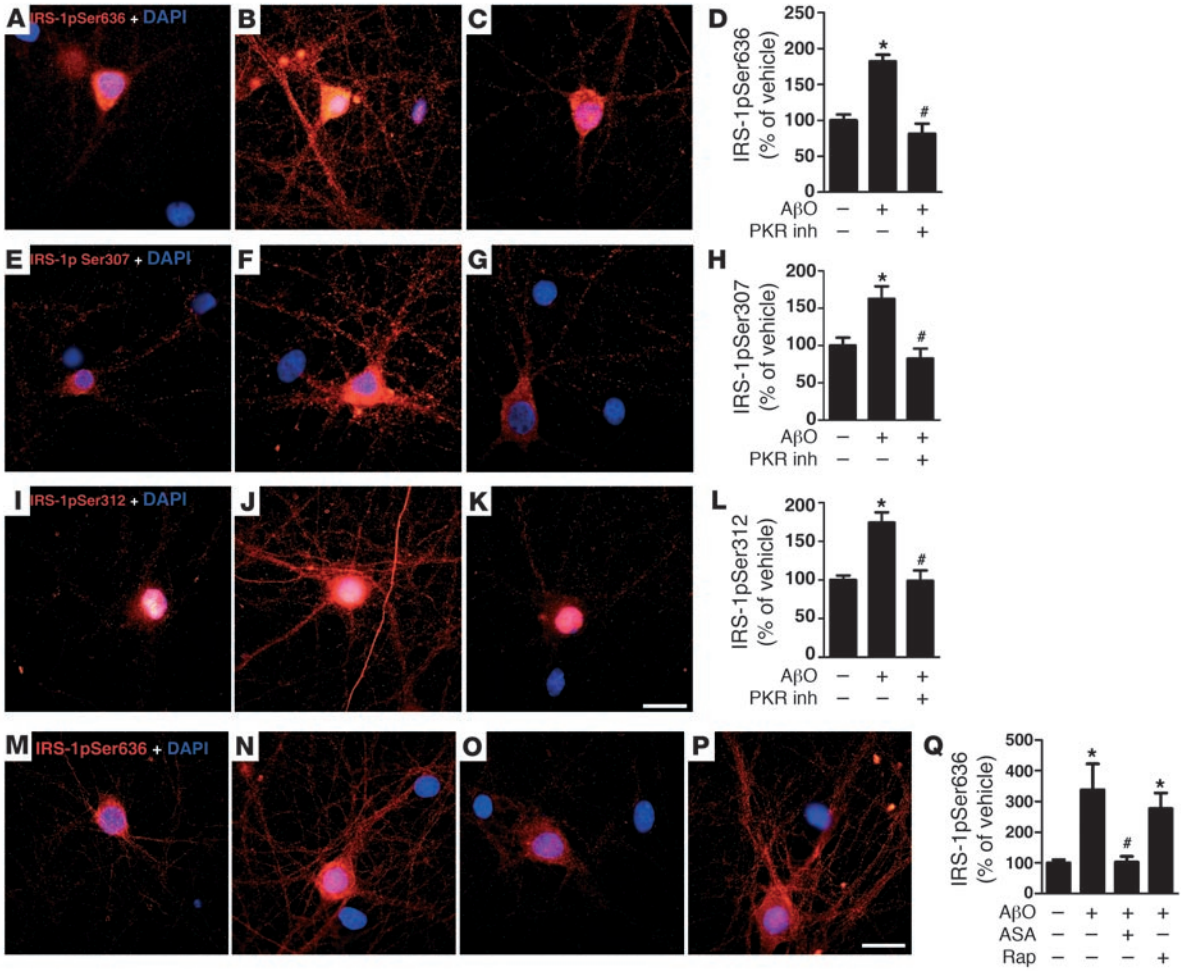

Figure 7

PKR and IKK, but not mTOR, mediate AβO-induced IRS-1pSer. (**A**–**Q**) Hippocampal neurons were exposed for 3 hours to vehicle (**A**, **E**, **I**, and **M**), 500 nM AβOs (**B**, **F**, **J**, and **N**), 1 μM PKR inhibitor (inh) plus 500 nM AβOs (**C**, **G**, and **K**), 5 mM acetylsalicylic acid (ASA) plus 500 nM AβOs (**O**), or 0.1 μM rapamycin (Rap) plus 500 nM AβOs (**P**). Scale bars: 50 μm. Integrated IRS-1pSer636 (**D** and **Q**), IRS-1pSer307 (**H**), and IRS-1pSer312 (**L**) immunofluorescence levels determined from 4 experiments using independent neuronal cultures (20 images analyzed per experimental condition per experiment). $^{*}P < 0.001$ relative to vehicle-treated cultures; $^{\#}P < 0.001$ relative to cultures exposed to AβOs; ANOVA followed by Bonferroni post-hoc test.

increased IRS-1pSer307. A recent study demonstrated that IRS-1pSer307 in mice is a positive regulatory site that sustains peripheral insulin signaling and moderates the severity of insulin resistance (65), in contrast to results obtained in previous cell-based experiments (26, 66, 67). Based on our results, it is likely that, following oligomer attack of synapses, the stress-sensitive kinases PKR, IKK, and JNK respond and coordinately lead to IRS-1pSer at multiple residues. Therefore, even if Ser307 is not phosphorylated, the final outcome may be that multiple serine-phosphorylated residues may act as critical regulators of neuronal insulin resistance, similar to what occurs in peripheral tissue (36).

Total IRS-2 levels were increased in hippocampal cultures exposed to AβOs. This might be related to the fact that, as previously observed, IRS-2 is a negative regulator of memory formation that acts by impairing dendritic spine formation (28) and that deletion of IRS-2 reduces amyloid deposition, cognitive deficits and premature mortality in Tg2576 mice (29). Beneficial effects of IRS-2 deletion in AD pathology parallel the effects on lifespan, with less IRS-2 signaling extending life span in mice (43). We found that IRS-2 levels were significantly decreased in APP/PS1 Tg mice compared with WT mice. Decreased levels of IRS-2 were also found in AD brains (4), suggesting a compensatory phenomenon to decrease the negative impact of brain IRS-2 signaling on memory in AD (68). So far, however, it is unclear whether this is an active neuroprotective response or a secondary response to the neurodegenerative process. Therefore, there is an apparent dichotomy between the neuroprotective effects of insulin signaling in CNS and its deleterious actions on lifespan and memory. It is possible that IRS-1 acts as a positive regulator of memory, as suggested by our current results, while IRS-2 acts as a negative modulator of memory formation.

AβOs increasingly appear to be the proximal toxins that cause synapse failure in AD (12, 13, 24, 25). Oligomers constitute key target for therapeutics, as drugs and antibodies designed to target them have provided positive results in AD clinical trials (69, 70). However, issues related to efficacy and safety of such approaches

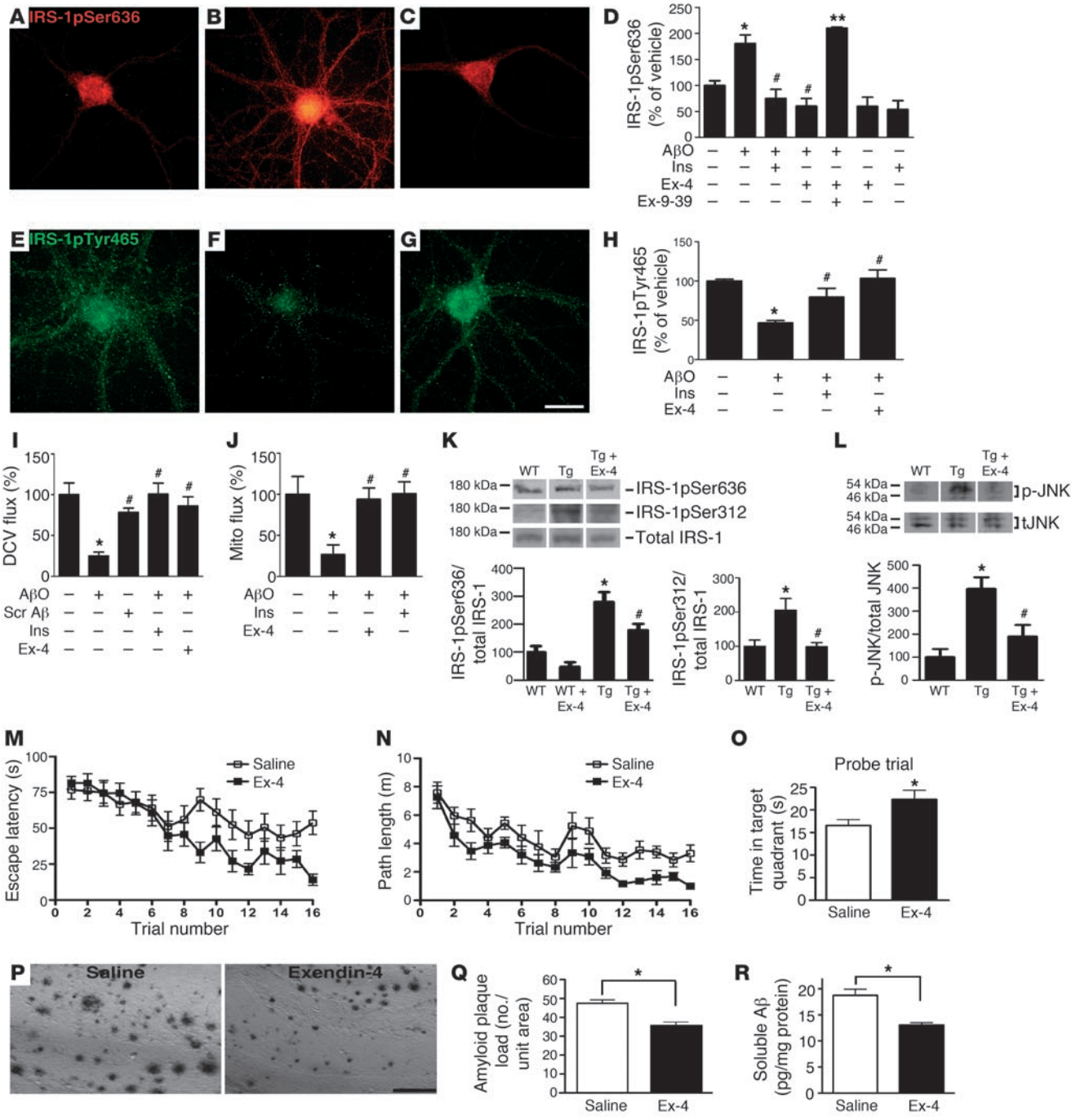

Figure 8

Exendin-4 prevents AβO-induced IRS-1pSer and p-JNK pathology and improves cognition in Tg mice. IRS-1pSer636 or IRS-1pTyr465 immunofluorescence of hippocampal neurons exposed for 3 hours to vehicle (**A** and **E**), 500 nM AβOs (**B** and **F**), 300 nM exendin-4 plus AβOs (**C** and **G**). Scale bar: 50 μm. Integrated IRS-1pSer636 (**D**) and IRS-1pTyr465 (**H**) immunofluorescence (4 independent experiments; 20 images analyzed/experimental condition/culture). **P* < 0.001, relative to vehicle-treated cultures; #*P* < 0.001, relative to AβO-exposed cultures; ***P* < 0.001, relative to cultures treated with exendin-4 plus AβOs. (**I** and **J**) Total DCV (**I**) and mitochondria (Mito; **J**) transport in neurons exposed to 500 nM AβOs, 300 nM exendin-4 plus AβOs, or 1 μM insulin plus AβOs for 18 hours (15 neurons/condition from ≥2 cultures were analyzed). **P* < 0.001 relative to vehicle-exposed cultures; #*P* < 0.001 relative to AβO-exposed cultures. (**K** and **L**) IRS-1pSer636, IRS-1pSer312, and p-JNK levels in hippocampi from 13-month-old WT mice (*n* = 5), vehicle-treated Tg mice (*n* = 7), or exendin-4–treated Tg mice (*n* = 5). Lanes were run on the same gel but were noncontiguous. Graphs show densitometric quantification of IRS-1pSer and p-JNK levels (normalized by total IRS-1 and JNK, respectively). **P* < 0.05 relative to WT; #*P* < 0.001 relative to vehicle-treated Tg mice; ANOVA followed by Bonferroni post-hoc test. (**M**–**O**) Exendin-4 improves spatial memory. (**M** and **N**) and memory retention (**O**) in the Morris water maze (10-month-old vehicle- or exendin-4–treated Tg mice were used; *n* = 12 in both groups). (**P** and **Q**) Brain amyloid plaque load (scale bar: 50 μm) and soluble Aβ levels (**R**) in vehicle- or exendin-4–treated APP/PS1 mice (*n* = 6, both groups; **P* < 0.05, Student's *t* test).

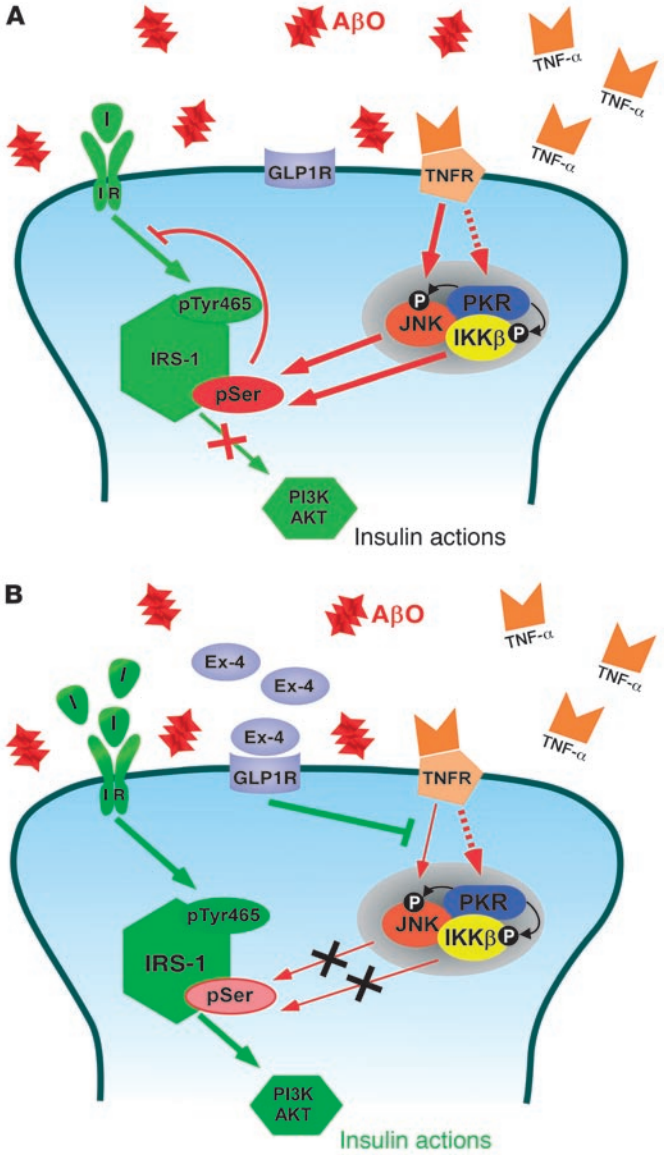

Figure 9
Proposed mechanism underlying disrupted brain insulin signaling in AD. (**A**) AβOs stimulate TNF-α signaling, which activates the JNK pathway and, possibly, PKR and IKK pathways. Activation of these stress-sensitive kinases, which can also be triggered by endoplasmic reticulum stress (36), results in serine phosphorylation of IRS-1, blocking downstream insulin signaling. (**B**) Stimulation of insulin and GLP1 receptors blocks AβO-induced defects in insulin signaling. Binding of exendin-4 to GLP1 receptors and of insulin to IRs prevented activation of JNK, allowing physiological tyrosine phosphorylation of IRS-1 and stimulating downstream insulin signaling. In both panels, red arrows indicate inhibitory pathways and green arrows indicate stimulatory pathways of insulin signaling. I, insulin.

have still not been fully addressed. Stimulation of neuronal insulin signaling has been proposed as a promising approach to prevent or halt memory decline in AD (41, 42). In vitro, insulin prevents AβO-induced loss of surface IRs, neuronal oxidative stress, and synapse deterioration (13). The mechanism of insulin protection involves IR signaling–dependent downregulation of oligomer binding to neurons. Thus, the protective action of insulin in rescuing the impairment of IRS-1 reported here probably derives from its ability to block oligomer binding to neurons. However, since IRs are removed from the neuronal membrane in AD brains (4) and in cultured neurons exposed to oligomers (9), use of insulin itself might not be the most effective way to combat AD. Instead, alternative approaches to bypass the IR and enhance insulin-related signaling pathways might provide a safe and effective strategy to prevent or treat AD. Here, we show that exendin-4, a novel antidiabetic drug that stimulates the insulin signaling pathway through activation of GLP1Rs, protected neurons against oligomer-induced dysregulation of IRS-1 phosphorylation (Figure 9B). Exendin-4 further decreased hippocampal IRS-1pSer and p-JNK levels, decreased amyloid pathology, and improved cognition in AD Tg mice. Enhancing brain insulin signaling through the use of exendin-4 or other GLP1R agonists may thus be a key alternative to block brain insulin resistance and memory impairment in AD.

Methods

Reagents

Synthetic $A\beta_{1-42}$ peptide was from American Peptide Co. Scrambled $A\beta_{1-42}$ was from Anaspec. Bovine and human insulin, 1,1,1,3,3,3,-hexafluoro-2-propanol (HFIP), DMSO, poly-L-lysine, rapamycin, and acetylsalicylic acid were from Sigma-Aldrich. Culture media/reagents, Alexa Fluor–labeled secondary antibodies, and ProLong anti-fade reagent were from Invitrogen. Electrophoresis buffers were from Bio-Rad. SuperSignal chemiluminescence reagents and the BCA protein assay kit were from Pierce. Antibodies against total IRS-1 and IRS-2, IRS-1pTyr465, IRS-1pSer636, glucagon-like peptide–1 receptor (GLP1R), TNFR1, TNF-α, and the PKR inhibitor were from Santa Cruz Biotechnology Inc. IRS-1pSer307, IRS-1pSer312, and IRS-1pSer616 antibodies were from Invitrogen. IRS-1pSer636/639 antibody for histology, the phosphorylated immunogen supplied as a custom order for specificity tests, glial fibrillary acidic protein (GFAP) antibody, p-JNK (Thr183/Tyr185) monoclonal antibody, and JNK polyclonal antibody were from Cell Signaling Technology. Unphosphorylated IRS-1 peptide (aa 631–646) was from Abcam (no. 41777). Exendin-4 and exendin 9-39 were from Bachem. SP600125 was from Tocris Bioscience.

Neuropathology in human brain tissue

NCI controls and patients with AD were autopsied with caregiver consent by the Center for Neurodegenerative Disease Research at the University of Pennsylvania. Clinical diagnosis of AD met NINCDS-ADRDA criteria and was confirmed by postmortem examination of the cerebral cortex and hippocampus for senile plaque and neurofibrillary tangle densities. A matched pairs design was used to match each of 22 AD cases with 22 NCI cases of the same sex, similar age (within 5 years), and similar postmortem interval (within 7 hours). Demographic and autopsy data on the subjects studied are given in Supplemental Table 1. Neither NCI controls nor AD patients had histories or symptoms of psychiatric conditions or non-AD neurological disorders.

At autopsy, each brain was cut into coronal slabs, from which an intermediate rostrocaudal segment of the hippocampal region (i.e., hippocampus, dentate gyrus, subiculum, and parahippocampal gyrus) was dissected and fixed in Bouin's fluid, 10% neutral buffered formalin, or 70% ethanol in saline for 24–48 hours. In each matched pair, the tissue sampled from the NCI and AD cases derived from the same hemisphere and was preserved in the same fixative. After being embedded in paraffin, 6-μm coronal sections were cut, mounted on slides, and reacted immunohistochemically

for IRS-1pSer636/639 with Cell Signaling Technology antibody 2388 at a dilution of 1:100 using an avidin-biotin-peroxidase method (71). Sections from all the case pairs were reacted together with the same solutions and exposure times to enable quantitative immunohistochemistry. A second set of sections from all pairs was run to test reliability of the results. After coverslipping and drying of the sections, the borders of hippocampal field CA1 were traced in ink on the slides under a dissecting scope aided by well-established criteria and atlas-style drawings (72). A series of ×100 photomicrographs covering all of CA1 in each section were then taken on a microscope with a motorized stage, and a composite montage was created using Image-Pro Plus software (Media Cybernetics Inc.). Photomicrographs of all NCI and AD sections were taken under the same lighting conditions. Image-Pro Plus was used to determine the area covered by CA1 in each section and the number of neurons with extranuclear IRS-1 pSer636/639 in that area by identifying immunoreactive objects that were larger in area than cell nuclei seen with hematoxylin staining and still within the size and shape parameters of neurons identified by NeuN immunoreactivity. The density of neurons with extranuclear IRS-1 pSer636/639 was then calculated. Five AD cases were tested for specificity of the IRS-1pSer636/639 antibody used in immunohistochemistry analyses (see Results).

AβOs and scrambled Aβ$_{1–42}$

Oligomers were prepared from synthetic Aβ$_{1–42}$ peptide (American Peptide) as previously described (16, 19). Scrambled Aβ peptide (Anaspec) treated in exactly the same manner was used in control experiments.

Mature hippocampal cultures

Primary rat hippocampal neuronal cultures were prepared according to established procedures (15, 16) and were used after 18–21 days in vitro (DIV). Cultures were prepared and maintained in Neurobasal medium supplemented with B-27, an insulin-containing supplement (Invitrogen). Some experiments (see Supplemental Figure 2) were performed using insulin-free B-27 (Invitrogen). Cultures were treated at 37°C for 3 hours with 500 nM AβOs or an equivalent volume of vehicle (2% DMSO in PBS). When present, insulin (1 μM), exendin-4 (300 nM), SP600125 (10 μM), infliximab (1 μg/ml), rapamycin (0.1 μM), and PKR inhibitor (1 μM) were added to cultures 30 minutes before AβOs. Acetylsalicylic acid (5 mM) was added to cultures 120 minutes before AβOs. Exendin 9-39 (1 μM) was added 15 minutes before exendin-4.

Immunocytochemistry

Cells were fixed and blocked as described previously (13, 15), incubated with AβO-selective NU4 mouse monoclonal antibody (16) and IRS-2, IRS-1, or p–IRS-1 (pSer636; pSer312; pSer616; pSer307; or pTyr465) rabbit polyclonal antibodies followed by Alexa Fluor–conjugated secondary antibodies. Coverslips were imaged on a Zeiss Axio Observer Z1 microscope.

Injections of AβOs into monkey brains and neuropathology studies

Four cynomolgus monkeys (*Macaca fascicularis*) aged 9 years (weight, 4.7–7.0 kg) were used. Animals were under the close supervision of a laboratory animal technician and the Queen's University veterinarian. AβOs were infused chronically through an i.c.v. canula. Three animals were administered 100 μg AβOs, every 3 days for 24 days. Oligomers were freshly prepared and characterized by size-exclusion chromatography (SEC) before each injection. One sham-operated animal, used as a control, had the cannula implanted into the lateral ventricle in the same manner as the experimental animals. At the end of the experimental protocol, animals were sedated with intramuscular 10 mg/kg ketamine with 0.01 mg/kg buprenorphine for analgesia, followed by intravenous 25 mg/kg sodium pentobarbital, perfused with PBS followed by 4% paraformaldehyde in PBS; 4% paraformaldehyde in PBS containing 2.5% glycerol; PBS plus 5% glycerol; and PBS plus 10% glycerol. Serial 40-μm-thick brain sections were obtained. Immunohistochemistry was performed using free-floating sections from hippocampus and temporal cortex in PBS containing 1% Triton incubated with 0.1 M citrate buffer, pH 6, at 60°C for 5 minutes. Sections were blocked with 5% BSA, 5% normal goat serum (NGS), and 1% Triton X-100 for 3 hours at room temperature. Primary antibodies (IRS-1pSer636, JNKpThr183/Tyr185, GFAP) were diluted in blocking solution, and sections were incubated overnight at 4°C, followed by incubation with Alexa Fluor–conjugated secondary antibodies for 2 hours at room temperature. Tissue autofluorescence was quenched by previous incubation with 0.06% potassium permanganate for 10 minutes at room temperature. Nuclei were stained with DAPI for 5 minutes. Slides were mounted with ProLong and imaged on a Zeiss Axio Observer Z1 microscope using structured illumination (ApoTome module) to decrease out-of-focus light.

AD Tg mouse model and treatment with exendin-4

APP/PS1 mice on a C57BL/6 background were obtained from The Jackson Laboratory. Mice not expressing the transgene were used as WT controls. Male animals were used in all studies. Animals were caged individually and maintained on a 12-hour light/12-hour dark cycle (lights on at 08:00, off at 20:00), in a temperature-controlled room (21.5 ± 1°C). Food and water were available ad libitum. Animals received daily intraperitoneal injections of exendin (25 nmol/kg, dissolved in saline) or vehicle (saline) during 3 weeks.

Western blot analysis of Tg mouse hippocampi and hippocampal neuronal cultures

Thirteen- to 14-month-old APP/PS1 Tg mice and WT control animals were used. Exendin-treated (n = 9) or vehicle-treated Tg (n = 7) and WT animals (n = 8) were euthanized. For Western immunoblot analysis, hippocampi of Tg mice and mature hippocampal cell cultures were homogenized in RIPA buffer containing protease and phosphatase inhibitor cocktails and resolved on a 4%–20% polyacrylamide gel with Tris/glycine/SDS buffer run at 125 V for 80 minutes at room temperature. The gel (42 μg total protein/lane) was electroblotted onto Hybond ECL nitrocellulose using 25 mM Tris, 192 mM glycine, 20% (v/v) methanol, 0.02% SDS, pH 8.3, at 350 mA for 2 hours at 4°C. Membranes were blocked with 5% nonfat milk in Tris-buffered saline containing Tween-20 (TBS-T) (0.1% Tween-20 in 20 mM Tris-HCl, pH 7.5, 0.8% NaCl) for 1 hour at room temperature. Primary antibodies (anti–IRS-1pSer636; pSer312; pSer307; pSer616 or anti–IRS-1 and anti–IRS-2 polyclonal antibodies [1:200], anti–p-JNK [Thr183/Tyr185] monoclonal antibody, anti-JNK polyclonal antibody [1:1,000], anti–TNF-α, anti-TNFR1, and anti-GLP1R polyclonal antibodies [1:200], or anti–cyclophilin B polyclonal antibody [1:10,000]) were diluted in 5% milk/TBS and incubated with the membranes for 120 minutes at room temperature. After incubation with HRP-conjugated anti-mouse or anti-rabbit IgGs (1:10,000 in TBS-T) for 60 minutes, membranes were washed, developed with SuperSignal West Femto Maximum Sensitivity substrate, and imaged on photographic film.

For TNF-α analysis, cultures were exposed to 500 nM AβOs or an equivalent volume of vehicle for 3 hours. The medium was then removed and concentrated by Speedvac (Savant Instruments Inc.) centrifugation. Protein concentrations were determined in the medium using the enhanced BCA protein assay kit (from Pierce). Samples containing equal protein amounts were resolved in a 4%–20% polyacrylamide gel, followed by Western blotting using anti–TNF-α antibody.

Data analysis

IRS-2, IRS-1, p–IRS-1(pSer636; pSer312; pSer616; pSer307; or pTyr465), and AβO binding immunofluorescence intensities were each analyzed in

3–6 experiments (see figure legends) using independent neuronal cultures. In each experiment, 20–30 images were acquired from 3 coverslips in each experimental condition. Histogram analysis of fluorescence intensities at each pixel across the images was performed using NIH ImageJ (http://rsbweb.nih.gov/ij/) as described previously (16). Cell bodies were digitally removed from the images so that only immunostaining on dendritic processes was quantified. Statistical significance was assessed by ANOVA followed by Bonferroni post-hoc test.

For neuropathology in monkey brains, IRS-1pSer636 and p-JNK immunolabeling densities were determined after proper thresholding using NIH ImageJ by counting the particles with diameters of 500 or fewer pixels and determining the total area (in pixels) occupied by particles in each field. For each animal, immunolabeling densities were measured in a set of 20–31 microscopic fields throughout the dentate gyrus or temporal cortex (see Results). Statistical significance was assessed by ANOVA followed by Bonferroni post-hoc test.

Plasmids and expression of transgenes

pβ-actin-BDNF-mRFP and pJPA5-YFP-JBD were from Gary Banker (Jungers Center for Neurosciences Research, Oregon Health and Science University, Portland, Oregon, USA). Mitochondrially targeted YFP was from Gordon Rintoul (Department of Biological Sciences, Simon Fraser University, Burnaby, British Columbia, Canada). Constructs were transfected into neurons at 9–12 DIV using Lipofectamine 2000 (Invitrogen). Cells were allowed to express constructs for 24 hours prior to exposure to AβOs and then imaged.

Live imaging

Cells were live imaged using a wide-field fluorescence microscope (DMI 6000 B, Leica), as described previously (35). Axons and dendrites were initially distinguished based on morphology and confirmed retrospectively by antibody staining against MAP-2, a dendritic cytoskeletal protein (73).

Videos and quantitative analyses

Videos were processed using MetaMorph (Universal Imaging) as described previously (35). Quantitative kymograph analysis was performed using MetaMorph.

Behavioral tests

Animals were handled daily for 2 weeks prior to commencement of the study. Mice were 9 months of age when treatment began. They received intraperitoneal exendin-4 (25 nmol/kg BW) or saline (0.9% w/v) injections twice daily for 3 weeks before behavioral tasks were conducted (n = 12 for each group). All experiments were licensed by the UK Home Office in accordance with the Animal (scientific procedures) Act of 1986.

Morris water maze task. The maze was made of white opaque plastic with a diameter of 120 cm and 40-cm-high walls and was filled with water at 25°C to avoid hypothermia. A small escape platform (10 × 6.5 × 21.5 cm) was placed at a fixed position in the center of one quadrant, 25 cm from the perimeter, and was hidden 1 cm beneath the water surface. The room contained a number of fixed visual cues on the walls.

Acquisition phase. The acquisition trial phase consisted of 4 training days and 4 trials per day with a 15-minute inter-trial interval. Four points equally spaced along the circumference of the pool (north, south, east, west) served as the starting position, which was randomized across the 4 trials each day. If an animal did not reach the platform within 90 seconds, it was guided to the platform, where it had to remain for 30 seconds, before being returned to its home cage. Mice were kept dry, between trials, in a plastic holding cage filled with paper towels. The path length and escape latencies were recorded (n = 12 per group).

Probe trial. One day after completion of the acquisition task (day 5), a probe trial was performed in order to assess spatial memory (after a 24-hour delay). The platform was removed from the maze, and animals were allowed to swim freely for 60 seconds. Spatial acuity was expressed as the amount of time spent in the exact area where the escape platform was located.

Histology in Tg mice

Mice were perfused transcardially with PBS buffer followed by ice-cold 4% paraformaldehyde in PBS. Brains were removed and fixed in 4% paraformaldehyde for at least 24 hours before being transferred to 30% sucrose solution overnight. Brains were then snap-frozen using Envirofreeze, and 40-μm-thick coronal sections were cut at coordinates bregma –2 to –3 using a Leica cryostat. Sections were chosen according to stereological rules (74), with the first section taken at random, followed by every fifth section afterward. Seven to 13 sections were analyzed per brain. Staining was carried out for Aβ plaques. All sections were incubated in 3% H_2O_2 to quench endogenous peroxidase activity. After the sections were blocked in 5% normal serum to avoid nonspecific antibody binding, they were incubated with rabbit polyclonal anti-Aβ peptide (1:250, Invitrogen 71-5800). After overnight incubation at 4°C, the sections were incubated in respective secondary antibodies. For visualization, Vectastain Elite and SG substrate (Vector Laboratories) were used. All staining was visualized by Axio Scope 1 (Zeiss) and analyzed using a multi-threshold plug-in with ImageJ, using stereological rules as described in ref. 75.

ELISA for total soluble Aβ levels

Soluble Aβ levels were measured using an ELISA kit (Invitrogen), used according to the manufacturer's instructions. Briefly, right hemispheres of control and exendin-4–treated APP/PS1 mouse brains were homogenized in Tris-buffered saline (25 mM Tris-HCl, pH 7.4, 150 mM NaCl) supplemented with protease inhibitor cocktail (Sigma-Aldrich, 250 μl per 5 ml buffer). Brain homogenates were centrifuged at 100,000 g and 4°C for 1 hour. The supernatant was then diluted 1:10 before the ELISA was carried out. Protein was quantified using the Bradford protein assay. Final soluble Aβ values were determined following normalization to total protein levels (n = 6 per group).

Statistics

Statistical analyses were performed (GraphPad Prism) using 2-tailed Student's t test when 2 conditions were compared and 1-way ANOVA followed by Bonferroni post-hoc test for multiple comparisons. Results are represented as mean ± SEM (unless stated otherwise), and the total number of independent experiments, as well as P values, are specified in each figure legend. P values less than 0.05 were considered significant.

Study approval

All experiments involving rats and Tg mice, unless otherwise specified, were performed in certified facilities under protocols approved by the Institutional Animal Care and Use Committee of the Federal University of Rio de Janeiro (protocols IBQM 022 and IBQM 019). All animal care and experimental procedures involving non-human primates were in accordance with the Canadian Council on Animal Care policies on the use of laboratory animals and approved by the Queen's University Animal Care Committee (Animal Care Protocol Original Munoz-2011-039-Or). For the human postmortem studies, informed consent was obtained for collection and use of clinical and postmortem data from all subjects of the present study or from their next-of-kin in accordance with the University of Pennsylvania's Institutional Review Board and its Alzheimer Disease Center (Clinical Core Protocol 068200).

Acknowledgments

This work was supported by the Human Frontier Science Program (HFSP) and the John Simon Guggenheim Memorial Foundation (FGF). F.G. De Felice and S.T. Ferreira are also funded by Conselho Nacional de Desenvolvimento Cientifico e Tecnológico (CNPq), Fundação de Amparo à Pesquisa do Estado do Rio de Janeiro (FAPERJ), and Instituto Nacional de Neurociência Translacional (INNT). T.R. Bomfim, L. Forny-Germano, L.B. Sathler, H.M. Melo, and J. Brito-Moreira are supported by predoctoral fellowships from Conselho Nacional de Desenvolvimento Cientifico e Tecnológico and Coordenação de Aperfeicoamento de Pessoal de Ensino Superior. Experiments on monkeys were funded by a grant (MOP-77734) from the Canadian Institutes of Health Research (to D.P. Munoz) and by HFSP (to F.G. De Felice). D.P. Munoz was also supported by the Canada Research Chair Program. W.L. Klein is funded by grants from the American Health Assistance Foundation, Alzheimer's Association, and NIH–National Institute on Aging grants R01-AG18877 and R01-AG22547. K. Talbot and S.E. Arnold were supported by a Temple Foundation Discovery award and by the Alzheimer's Association. M.A. Silverman is funded by the National Science and Engineering Research Council (no. 327100-06), the Canadian Foundation for Innovation (12793), and the Canadian Institutes of Health Research (no. 90396). We thank G. Banker (Oregon Health State University) for the gift of DN JNK and L. Veloso (University of Campinas, Campinas, Brazil) for the gift of infliximab.

Received for publication January 26, 2011, and accepted in revised form January 5, 2012.

Address correspondence to: Fernanda G. De Felice, Institute of Medical Biochemistry, CCS, Room H2-019, Federal University of Rio de Janeiro, Rio de Janeiro, RJ 21944-590, Brazil. Phone: 5521.2562.6790; Fax: 5521.2270.8647; E-mail: felice@bioqmed.ufrj.br.

1. White MF. IRS proteins and the common path to diabetes. *Am J Physiol Endocrinol Metab*. 2002; 283(3):E413–E422.
2. Craft S. Insulin resistance and Alzheimer's disease pathogenesis: potential mechanisms and implications for treatment. *Curr Alzheimer Res*. 2007; 4(2):147–152.
3. de la Monte SM. Insulin resistance and Alzheimer's disease. *BMB Rep*. 2009;42(8):475–481.
4. Moloney AM, Griffin RJ, Timmons S, O'Connor R, Ravid R, O'Neill C. Defects in IGF-1 receptor, insulin receptor and IRS-1/2 in Alzheimer's disease indicate possible resistance to IGF-1 and insulin signalling. *Neurobiol Aging*. 2010;31(2):224–243.
5. Steen E, et al. Impaired insulin and insulin-like growth factor expression and signaling mechanisms in Alzheimer's disease — is this type 3 diabetes? *J Alzheimers Dis*. 2005;7(1):63–80.
6. Lester-Coll N, Rivera EJ, Soscia SJ, Doiron K, Wands JR, de la Monte SM. Intracerebral streptozotocin model of type 3 diabetes: relevance to sporadic Alzheimer's disease. *J Alzheimers Dis*. 2006;9(1):13–33.
7. Chiu SL, Chen CM, Cline HT. Insulin receptor signaling regulates synapse number, dendritic plasticity, and circuit function in vivo. *Neuron*. 2008; 58(5):708–719.
8. Dou JT, Chen M, Dufour F, Alkon DL, Zhao WQ. Insulin receptor signaling in long-term memory consolidation following spatial learning. *Learn Mem*. 2005;12(6):646–655.
9. Zhao WQ, et al. Amyloid beta oligomers induce impairment of neuronal insulin receptors. *FASEB J*. 2008;22(1):246–260.
10. Haass C, Selkoe DJ. Soluble protein oligomers in neurodegeneration: lessons from the Alzheimer's amyloid beta-peptide. *Nat Rev Mol Cell Biol*. 2007; 8(2):101–112.
11. Ferreira ST, Vieira MN, De Felice FG. Soluble protein oligomers as emerging toxins in Alzheimer's and other amyloid diseases. *IUBMB Life*. 2007;59(4–5):332–345.
12. Ferreira ST, Klein WL. The Abeta oligomer hypothesis for synapse failure and memory loss in Alzheimer's disease. *Neurobiol Learn Mem*. 2011; 96(4):529–543.
13. De Felice FG, et al. Protection of synapses against Alzheimer's-linked toxins: insulin signaling prevents the pathogenic binding of Abeta oligomers. *Proc Natl Acad Sci U S A*. 2009;106(6):1971–1976.
14. Gong Y, et al. Alzheimer's disease-affected brain: presence of oligomeric A beta ligands (ADDLs) suggests a molecular basis for reversible memory loss. *Proc Natl Acad Sci U S A*. 2003;100(18):10417–10422.
15. De Felice FG, et al. Alzheimer's disease-type neuronal tau hyperphosphorylation induced by A beta oligomers. *Neurobiol Aging*. 2008;29(9):1334–1347.
16. De Felice FG, et al. Abeta oligomers induce neuronal oxidative stress through an N-methyl-D-aspartate receptor-dependent mechanism that is blocked by the Alzheimer drug memantine. *J Biol Chem*. 2007;282(15):11590–11601.
17. Decker H, et al. N-methyl-D-aspartate receptors are required for synaptic targeting of Alzheimer's toxic amyloid-beta peptide oligomers. *J Neurochem*. 2010;115(6):1520–1529.
18. Lacor PN, et al. Abeta oligomer-induced aberrations in synapse composition, shape, and density provide a molecular basis for loss of connectivity in Alzheimer's disease. *J Neurosci*. 2007;27(4):796–807.
19. Lambert MP, et al. Diffusible, nonfibrillar ligands derived from Abeta1-42 are potent central nervous system neurotoxins. *Proc Natl Acad Sci U S A*. 1998;95(11):6448–6453.
20. Townsend M, Mehta T, Selkoe DJ. Soluble Abeta inhibits specific signal transduction cascades common to the insulin receptor pathway. *J Biol Chem*. 2007;282(46):33305–33312.
21. Escribano L, et al. Rosiglitazone rescues memory impairment in Alzheimer's transgenic mice: mechanisms involving a reduced amyloid and tau pathology. *Neuropsychopharmacology*. 2010;35(7):1593–1604.
22. Hirosumi J, et al. A central role for JNK in obesity and insulin resistance. *Nature*. 2002;420(6913):333–336.
23. Hotamisligil GS, Peraldi P, Budavari A, Ellis R, White MF, Spiegelman BM. IRS-1-mediated inhibition of insulin receptor tyrosine kinase activity in TNF-alpha- and obesity-induced insulin resistance. *Science*. 1996;271(5249):665–668.
24. Shankar GM, et al. Amyloid-beta protein dimers isolated directly from Alzheimer's brains impair synaptic plasticity and memory. *Nat Med*. 2008; 14(8):837–842.
25. Lesne S, et al. A specific amyloid-beta protein assembly in the brain impairs memory. *Nature*. 2006; 440(7082):352–357.
26. Rui L, et al. Insulin/IGF-1 and TNF-alpha stimulate phosphorylation of IRS-1 at inhibitory Ser307 via distinct pathways. *J Clin Invest*. 2001;107(2):181–189.
27. Brewer GJ, Boehler MD, Jones TT, Wheeler BC. NbActiv4 medium improvement to Neurobasal/B27 increases neuron synapse densities and network spike rates on multielectrode arrays. *J Neurosci Methods*. 2008;170(2):181–187.
28. Irvine EE, et al. Insulin receptor substrate 2 is a negative regulator of memory formation. *Learn Mem*. 2011;18(6):375–383.
29. Killick R, et al. Deletion of Irs2 reduces amyloid deposition and rescues behavioural deficits in APP transgenic mice. *Biochem Biophys Res Commun*. 2009; 386(1):257–262.
30. Bouzakri K, et al. Reduced activation of phosphatidylinositol-3 kinase and increased serine 636 phosphorylation of insulin receptor substrate-1 in primary culture of skeletal muscle cells from patients with type 2 diabetes. *Diabetes*. 2003;52(6):1319–1325.
31. Ma QL, et al. Beta-amyloid oligomers induce phosphorylation of tau and inactivation of insulin receptor substrate via c-Jun N-terminal kinase signaling: suppression by omega-3 fatty acids and curcumin. *J Neurosci*. 2009;29(28):9078–9089.
32. Cacquevel M, Lebeurrier N, Cheenne S, Vivien D. Cytokines in neuroinflammation and Alzheimer's disease. *Curr Drug Targets*. 2004;5(6):529–534.
33. Morfini GA, et al. Pathogenic huntingtin inhibits fast axonal transport by activating JNK3 and phosphorylating kinesin. *Nat Neurosci*. 2009;12(7):864–871.
34. Morfini GA, et al. Axonal transport defects in neurodegenerative diseases. *J Neurosci*. 2009; 29(41):12776–12786.
35. Decker H, Lo KY, Unger SM, Ferreira ST, Silverman MA. Amyloid-beta peptide oligomers disrupt axonal transport through an NMDA receptor-dependent mechanism that is mediated by glycogen synthase kinase 3beta in primary cultured hippocampal neurons. *J Neurosci*. 2010;30(27):9166–9171.
36. Nakamura T, et al. Double-stranded RNA-dependent protein kinase links pathogen sensing with stress and metabolic homeostasis. *Cell*. 2010;140(3):338–348.
37. Yuan M, et al. Reversal of obesity- and diet-induced insulin resistance with salicylates or targeted disruption of Ikkbeta. *Science*. 2001;293(5535):1673–1677.
38. Cai D, et al. Local and systemic insulin resistance resulting from hepatic activation of IKK-beta and NF-kappaB. *Nat Med*. 2005;11(2):183–190.
39. Hundal RS, et al. Mechanism by which high-dose aspirin improves glucose metabolism in type 2 diabetes. *J Clin Invest*. 2002;109(10):1321–1326.
40. Ozes ON, et al. A phosphatidylinositol 3-kinase/Akt/mTOR pathway mediates and PTEN antagonizes tumor necrosis factor inhibition of insulin signaling through insulin receptor substrate-1. *Proc Natl Acad Sci U S A*. 2001;98(8):4640–4645.
41. Dhamoon MS, Noble JM, Craft S. Intranasal insulin improves cognition and modulates beta-amyloid in early AD. *Neurology*. 2009;72(3):292–293.
42. Benedict C, Hallschmid M, Schultes B, Born J, Kern W. Intranasal insulin to improve memory function in humans. *Neuroendocrinology*. 2007;86(2):136–142.
43. Taguchi A, White MF. Insulin-like signaling, nutrient homeostasis, and life span. *Annu Rev Physiol*. 2008;70:191–212.
44. During MJ, et al. Glucagon-like peptide-1 receptor is involved in learning and neuroprotection. *Nat Med*. 2003;9(9):1173–1179.
45. Cole GM, Frautschy SA. The role of insulin and neurotrophic factor signaling in brain aging and Alzheim-

er's disease. *Exp Gerontol*. 2007;42(1–2):10–21.
46. Mattson MP, Perry T, Greig NH. Learning from the gut. *Nat Med*. 2003;9(9):1113–1115.
47. McClean PL, Gault VA, Harriott P, Holscher C. Glucagon–like peptide–1 analogues enhance synaptic plasticity in the brain: a link between diabetes and Alzheimer's disease. *Eur J Pharmacol*. 2010; 630(1–3):158–162.
48. Toledo EM, Inestrosa NC. Activation of Wnt signaling by lithium and rosiglitazone reduced spatial memory impairment and neurodegeneration in brains of an APPswe/PSEN1DeltaE9 mouse model of Alzheimer's disease. *Mol Psychiatry*. 2010;15(3):272–285.
49. Ferdaoussi M, et al. Exendin-4 protects beta-cells from interleukin-1 beta-induced apoptosis by interfering with the c-Jun NH2-terminal kinase pathway. *Diabetes*. 2008;57(5):1205–1215.
50. Natalicchio A, et al. Exendin-4 prevents c-Jun N-terminal protein kinase activation by tumor necrosis factor-alpha (TNFalpha) and inhibits TNFalpha-induced apoptosis in insulin-secreting cells. *Endocrinology*. 2010;151(5):2019–2029.
51. Janson J, Laedtke T, Parisi JE, O'Brien P, Petersen RC, Butler PC. Increased risk of type 2 diabetes in Alzheimer disease. *Diabetes*. 2004;53(2):474–481.
52. Carlson CJ, White MF, Rondinone CM. Mammalian target of rapamycin regulates IRS-1 serine 307 phosphorylation. *Biochem Biophys Res Commun*. 2004;316(2):533–539.
53. Fisher TL, White MF. Signaling pathways: the benefits of good communication. *Curr Biol*. 2004; 14(23):R1005–R1007.
54. Lafay-Chebassier C, et al. mTOR/p70S6k signalling alteration by Abeta exposure as well as in APP-PS1 transgenic models and in patients with Alzheimer's disease. *J Neurochem*. 2005;94(1):215–225.
55. Caccamo A, Majumder S, Richardson A, Strong R, Oddo S. Molecular interplay between mammalian target of rapamycin (mTOR), amyloid-beta, and Tau: effects on cognitive impairments. *J Biol Chem*. 2010;285(17):13107–13120.
56. Spilman P, et al. Inhibition of mTOR by rapamycin abolishes cognitive deficits and reduces amyloid-beta levels in a mouse model of Alzheimer's disease. *PLoS One*. 2010;5(4):e9979.
57. Ma T, et al. Dysregulation of the mTOR pathway mediates impairment of synaptic plasticity in a mouse model of Alzheimer's disease. *PLoS One*. 2010; 5(9):e12845.
58. Morel M, Couturier J, Lafay-Chebassier C, Paccalin M, Page G. PKR, the double stranded RNA-dependent protein kinase as a critical target in Alzheimer's disease. *J Cell Mol Med*. 2009;13(8A):1476–1488.
59. Selkoe DJ. Resolving controversies on the path to Alzheimer's therapeutics. *Nat Med*. 2011; 17(9):1060–1065.
60. Hotamisligil GS, Murray DL, Choy LN, Spiegelman BM. Tumor necrosis factor alpha inhibits signaling from the insulin receptor. *Proc Natl Acad Sci U S A*. 1994;91(11):4854–4858.
61. Uysal KT, Wiesbrock SM, Marino MW, Hotamisligil GS. Protection from obesity-induced insulin resistance in mice lacking TNF-alpha function. *Nature*. 1997;389(6651):610–614.
62. Wiedmann MW, Mossner J, Baerwald C, Pierer M. TNF alpha inhibition as treatment modality for certain rheumatologic and gastrointestinal diseases. *Endocr Metab Immune Disord Drug Targets*. 2009; 9(3):295–314.
63. Araujo EP, et al. Infliximab restores glucose homeostasis in an animal model of diet-induced obesity and diabetes. *Endocrinology*. 2007;148(12):5991–5997.
64. Tobinick E. Perispinal etanercept: a new therapeutic paradigm in neurology. *Expert Rev Neurother*. 2010;10(6):985–1002.
65. Copps KD, Hancer NJ, Opare-Ado L, Qiu W, Walsh C, White MF. Irs1 serine 307 promotes insulin sensitivity in mice. *Cell Metab*. 2010;11(1):84–92.
66. Aguirre V, Uchida T, Yenush L, Davis R, White MF. The c-Jun NH(2)-terminal kinase promotes insulin resistance during association with insulin receptor substrate-1 and phosphorylation of Ser(307). *J Biol Chem*. 2000;275(12):9047–9054.
67. Aguirre V, Werner ED, Giraud J, Lee YH, Shoelson SE, White MF. Phosphorylation of Ser307 in insulin receptor substrate-1 blocks interactions with the insulin receptor and inhibits insulin action. *J Biol Chem*. 2002;277(2):1531–1537.
68. Freude S, et al. Neuronal IGF-1 resistance reduces Abeta accumulation and protects against premature death in a model of Alzheimer's disease. *FASEB J*. 2009;23(10):3315–3324.
69. Klyubin I, et al. Amyloid beta protein immunotherapy neutralizes Abeta oligomers that disrupt synaptic plasticity in vivo. *Nat Med*. 2005;11(5):556–561.
70. Relkin NR, et al. 18-Month study of intravenous immunoglobulin for treatment of mild Alzheimer disease. *Neurobiol Aging*. 2009;30(11):1728–1736.
71. Talbot K, et al. Dysbindin-1 is reduced in intrinsic, glutamatergic terminals of the hippocampal formation in schizophrenia. *J Clin Invest*. 2004; 113(9):1353–1363.
72. Amaral DG, Insausti R, Campbell MJ. Distribution of somatostatin immunoreactivity in the human dentate gyrus. *J Neurosci*. 1988;8(9):3306–3316.
73. Kwinter DM, Lo K, Mafi P, Silverman MA. Dynactin regulates bidirectional transport of dense-core vesicles in the axon and dendrites of cultured hippocampal neurons. *NeuroScience*. 2009;162(4):1001–1010.
74. Bondolfi L, et al. Amyloid-associated neuron loss and gliogenesis in the neocortex of amyloid precursor protein transgenic mice. *J Neurosci*. 2002;22(2):515–522.
75. Gengler S, McClean PL, McCurtin R, Gault VA, Hölscher C. Val(8)GLP–1 rescues synaptic plasticity and reduces dense core plaques in APP/PS1 mice. *Neurobiol Aging*. 2012;33(2):265–276.